Article

Dielectric Barrier Discharge Coupling Catalytic Oxidation for Highly Efficient Hg^0 Conversion

Yujie Liao, Zhong Zhong, Shaoping Cui, Dong Fu, and Pan Zhang*

Read Online

ACCESS | Metrics & More | Article Recommendations

ABSTRACT: In this work, we prepared CuCe/Ti catalysts in a dielectric barrier discharge (DBD) reactor and proposed a new method for flue gas mercury oxidation using DBD coupling CuCe/Ti catalyst. Our experiments verified the oxidation efficiency of flue gas Hg^0 (η_{Hg}) and clarified the influence of O$_2$ content, NO concentration, SO$_2$ concentration, water vapor content, and discharge voltage on η_{Hg}. The oxidation mechanism of Hg^0 in the DBD-CuCe/Ti reactor was also illustrated. The Hg^0 oxidation experiment on the simulated flue gas (70 μg/m^3 Hg^0 + 300 mg/m^3 NO + 1000 mg/m^3 SO$_2$ + 6%O$_2$) with a flow rate of 1 L/min showed that when the amount of catalyst was 1.25 g and the discharge voltage was 9.5 kV, a η_{Hg} of 93% can be achieved, which indicates that the DBD coupling CuCe/Ti technology is suitable for Hg^0 conversion and flue gas mercury removal.
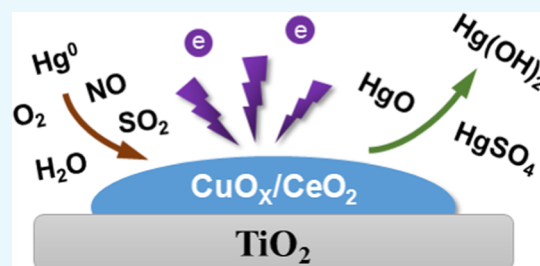
1. INTRODUCTION

The mercury in the environment can be divided into naturally released mercury and human released mercury. Eighty percent of the mercury in the atmosphere is in the form of vapor, and mainly from the burning of fossil fuels. Gaseous mercury is mercury that can pass through a 0.45 μm pore filter membrane or other filtering devices. It has the characteristics of long retention time, so it can not only carry out the long-distance transmission but also participate in the global mercury cycle, form particles, and settle in situ. China is the world's largest coal consumer. The average mercury content (approximately 0.15−0.20 μg/g) of coal in China is higher than the world averaged content (0.13 μg/g), thus the mercury pollution problem in China is more serious.[1−4]

The Hg in coal mainly exists in the form of mercury−sulfur bonds. When the boiler burns at high temperatures, the mercury−sulfur bond breaks, and most of the Hg enters into the flue gas in the form of gaseous element mercury Hg^0, which may be chlorinated or oxidized to form Hg^{2+} or be catalytically oxidized on the surface of fly ash. Gaseous Hg^{2+} is adsorbed on the surface of fly ash to form particulate mercury Hg$_p$.[5,65,6] At present, there are three ways to remove mercury after combustion. One is to modify the existing flue gas purification equipment to achieve the combined removal of multiple pollutants and improve the removal efficiency; the other is to add absorbents to the tail flue gas to remove Hg; the third is to use a catalyst to oxidize Hg in the flue gas to ease its removal.[7−10] For example, selective catalytic reduction (SCR) technology can oxidize Hg^0 to Hg^{2+} and the conversion rate reaches 30−80%.[11] The generated Hg^{2+} and particulate mercury Hg$_p$ can be further removed by electro-

static precipitator (ESP) or bag filter and wet desulfurization unit. However, these traditional mercury removal methods have too long and complicated processes, numerous equipment, and a large area occupation, and the operation and equipment maintenance costs are too high.[12] Therefore, the development of new technologies and the use of as few equipment as possible to efficiently remove multiple pollutants in a relatively short process are important development directions for flue gas purification.[10,13]

Hg^0 has a low melting point and is not easily soluble in water, acid, and alkali. Therefore, the removal of Hg^0 depends on its efficient and quick oxidation of Hg^0 to Hg^{2+}, which is easily removed.[14] The use of nonthermal plasma (NTP) to treat the catalyst and then coordinate Hg^0 removal will be one of the new development trends of flue gas Hg^0 removal in the future. Compared with the traditional Hg^0 removal technology, this method can not only save the cost of the precious metal catalyst but also efficiently remove a variety of pollutants in the flue gas. Moreover, it has a small equipment area, simple procedures, operation convenience, and other advantages.[15]

NTP uses corona discharge to generate $^\bullet$O and $^\bullet$OH free radical particles and O$_3$, which has a good effect on the
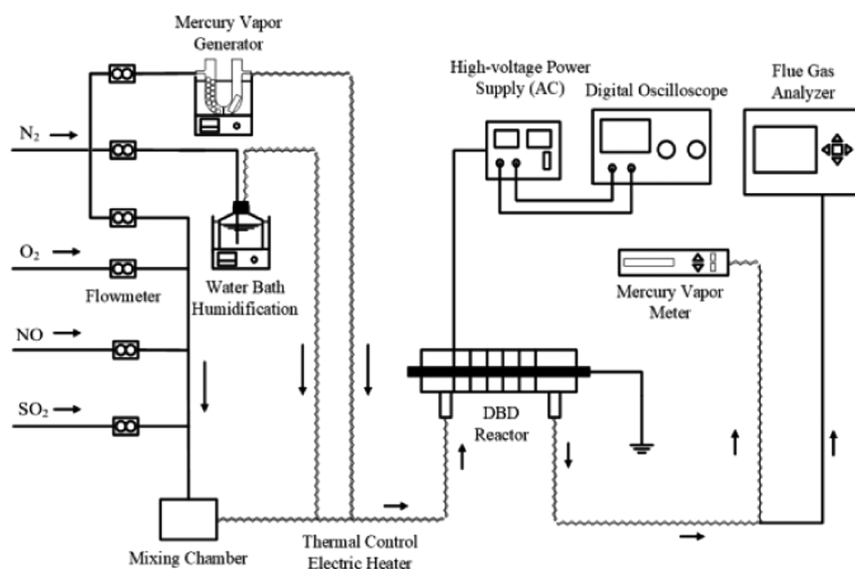
Figure 1. Experimental system schematic.

oxidation of pollutants such as NO, SO_2, and Hg^0. Studies have shown[16,17] that NTP effectively removes NO, SO_2, and Hg^0 in the flue gas, but there are also some problems, such as large power consumption, low selectivity of active free radicals, and low energy utilization efficiency.[8,18,19] Therefore, other approaches must be combined to promote the application of NTP technology in the pollutant removal process. Catalytic oxidation is one of the commonly used approaches because it can increase the reaction rate and promote the conversion of pollutants. In this approach, the role of the catalyst is very critical.[20,21] Commonly used catalysts include precious metals, transition-metal oxides, activated carbon, and molecular sieves. In recent years, catalysts loading transition-metal oxides such as iron, copper, manganese, cobalt, and cerium have been extensively studied.[22,23] An et al.[24] prepared a 3% CeO_2-WO_3/TiO_2 catalyst and found that the oxidation efficiency of Hg^0 (η_{Hg}) can reach 86.6% after combining with NTP.

Plasma technology has the advantage of the ability to produce nanostructured catalysts, low energy consumption, environmentally friendly properties, ability to use a wide range of substrates, and a high degree of universality in catalyst preparation compared with calcination.[25,26]

Liu et al.[12] and Huang et al.[27] showed that the catalyst with good performance could be prepared in a dielectric barrier discharge (DBD) reactor. When the catalyst is filled in the discharge area of DBD, the performance of the catalyst can be further improved in the discharge process of DBD.[28] Our previous work[29−31] showed that DBD combined with the catalyst can effectively promote simultaneous oxidation. Zhang et al.[32] and Zhou et al.[33] showed that the DBD coupling catalyst can significantly improve η_{Hg}. Previous studies[29−31] have also shown that, compared with other metal oxides, Cu oxide has a strong ability to oxidize Hg^0, while Ce oxide has good oxygen storage capacity. Titanium dioxide (TiO_2) is rich in resources, has low cost, has stable chemical properties, and resistant to acid and alkali corrosion, thus it is often used as a synthetic material for commercial catalysts. It can be expected that the TiO_2 catalyst loaded with Cu oxide and Ce oxide has a good oxidation ability for Hg^0. Therefore, the combination of DBD-CuCe/Ti catalyst is worthy of further study.[34−36]

The main contents of this work are as follows: (1) use DBD reactor to prepare a CuCe/Ti catalyst suitable for Hg^0 oxidation and perform X-ray diffraction (XRD) pattern analysis, X-ray photoelectron (XPS) energy spectrum analysis, and scanning electron microscopy (SEM) analysis; (2) determine the oxidation and conversion efficiency of Hg^0 by the DBD-CuCe/Ti reactor and show the influence of O_2 content, NO concentration, SO_2 concentration, and water vapor content on η_{Hg}; and (3) clarify the oxidation mechanism in the DBD-CuCe/Ti reactor.

2. EXPERIMENTAL SECTION

2.1. Chemicals and Materials. Cerium nitrate solution ($Ce(NO_3)_3\cdot6H_2O$) and copper nitrate ($Cu(NO_3)_2\cdot3H_2O$) were of AR grade and purchased from Shanghai Macklin Biochemical Co., Ltd. Titanium dioxide (TiO_2, P25) was purchased from Degussa. All chemicals were used as received without further purification. The deionized water used in the experiment was prepared with an ultrapure system. High-purity N_2, high-purity O_2, 5% NO/N_2, and 5% SO_2/N_2 were used as plasma-catalytic reaction reactants.

2.2. Catalyst Preparation. Using TiO_2 (Degussa P25) as a carrier, the required catalyst was prepared by the impregnation method. To prepare Cu/Ti (mass ratio Cu/TiO_2 = 0.1), Ce/Ti (mass ratio Ce/TiO_2 = 0.1), and CuCe/Ti (molar ratio Cu/Ce = 1:1, mass ratio (Cu + Ce)/TiO_2 = 0.1) catalysts, $Cu(NO_3)_2\cdot3H_2O$ and $Ce(NO_3)_3\cdot6H_2O$ were needed. First, certain amounts of cerium nitrate and copper nitrate were dissolved in deionized water then the dried TiO_2 (Degussa P25) powder was added into the solution. The mixture was stirred using a thermostatic magnetic stirrer (DF101S, Yuhua Instrument Company, Gongyi) at a constant temperature of 60 °C for 30 min. Subsequently, the sample was sonicated with an ultrasonic oscillator (PS-30T, Kangjie Electric Appliance Company, Shenzhen) for 30 min. Finally, the catalyst precursor was packed in the sealed discharge area of the DBD reactor, then N_2 and O_2 were passed into the reactor through a gas distribution system. DBD discharged the catalyst precursor under N_2-O_2 atmosphere to prepare the required catalyst.

2.3. Catalyst Characterization. The crystal morphology of the catalyst was determined by an X-ray diffractometer (D8, Bruker, Germany). The diffractometer used Cu Kα (λ = 0.1542 nm) as the radiation source, with a diffraction angle of 2θ ranging from 10 to 90° and a resolution of 0.02°. The results were analyzed by MDI Jade 6.0 software. X-ray photoelectron spectroscopy (XPS) analysis was performed on an electron spectrometer (ESCALAB 250 Xi, Thermo Scientific). All binding energies were calibrated by the C 1s line of 284.6 eV. The relative content of the elements on the catalyst surface was deduced by analysis and fitting of the Gaussian−Lorentzian curves using XPS PEAK software. Scanning electron microscopy (SEM) images were taken on a JEOL JSM-7500F instrument equipped with an OXFORD energy-dispersive spectrometer at an acceleration voltage.

2.4. Experimental Setup. The system shown in Figure 1 can be used to prepare the catalysts and oxidize pollutants. The whole system is divided into the gas distribution system, DBD reactor, discharge control and monitoring system, analysis and test system, and exhaust gas treatment system.

The simulated flue gas was prepared by the gas distribution system, and the N_2, NO, SO_2, and O_2 gases were mixed according to the required concentration under the control of the flowmeter. $H_2O(g)$ was produced by a water vapor generator. The mercury permeation tube was placed in a U-shaped glass tube filled with glass beads, which ensured uniform heating of the mercury permeation tube and a uniform gas flow. The U-shaped tube was heated in a water bath at a constant temperature (50 °C) to ensure a stable amount of elemental mercury (70 $\mu g/m^3$). The catalyst (1.25 g) was placed in the discharge space of the DBD reactor and fixed by quartz wool. The flow rate of the inlet flue gas was 1 L/min. The reacted gas was analyzed by a mercury analyzer and a flue gas analyzer and finally emptied after being absorbed by an exhaust gas treatment device.

3. RESULTS AND DISCUSSION

3.1. XRD, XPS, and SEM Analysis. The XRD patterns of the Cu/Ti, Ce/Ti, and CuCe/Ti catalysts are shown in Figure 2. The observed characteristic peaks of CuO/Cu_2O (Cu/Ti catalyst), CeO_2 (Ce/Ti catalyst), $CuO/Cu_2O/CeO_2$ (CuCe/Ti catalyst) indicated that the CuCe/Ti catalyst had a higher dispersion of Cu and Ce oxides. Moreover, the crystallinity of
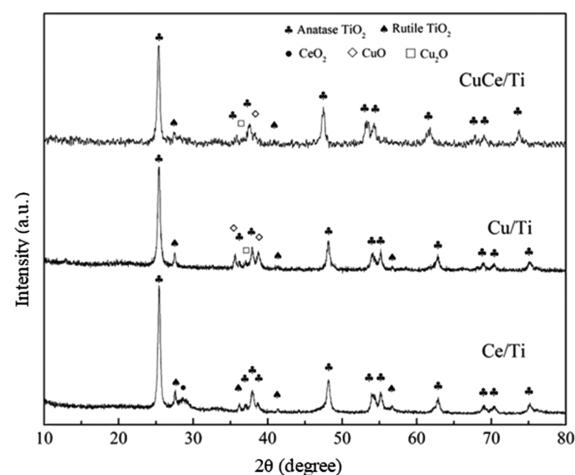
Cu and Ce oxides in the CuCe/Ti catalyst was lower. A study showed that the active component oxide with low crystallinity is more favorable for the catalytic reaction.[37] Therefore, the catalytic oxidation activity of the catalyst containing CuCe may be higher.

The photoelectron spectra of Cu 2p, Ce 3d, O 1s, and Ti 2p are shown in Figure 3. From Figure 3a, it can be observed that $Cu^{2+}/(Cu^+ + Cu^{2+})$ in Cu/Ti and CuCe/Ti were 70.6 and 76.2%, respectively. Cu^{2+} is an active site, which can strengthen the oxidation of Hg^0, thereby promoting the catalytic oxidation under low-temperature conditions.[38] The proportions of $Ce^{3+}/(Ce^{3+} + Ce^{4+})$ in Cu/Ti and in CuCe/Ti obtained from Figure 3b are 28.3 and 31.1%, respectively. The doped Cu and Ce may decrease the energy required for the formation of oxygen vacancies on the catalyst surface, increasing $Ce^{3+}/(Ce^{3+} + Ce^{4+})$, which is conducive to the formation of chemisorbed oxygen. From Figure 3c, it can be calculated that $O_\alpha/(O_\alpha + O_\beta)$ in CuCe/Ti is 25.4%, while these values in Ce/Ti and Cu/Ti are 15.3 and 16.9%, respectively. Therefore, CuCe/Ti may have higher catalytic activity in the catalytic oxidation of Hg^0.[39] It can be calculated from Figure 3d that the values of $Ti^{3+}/(Ti^{3+} + Ti^{4+})$ in Ce/Ti, Cu/Ti, and CuCe/Ti are 68.6, 70.6, and 77.2%, respectively. As active O species have mainly resulted from the conversion of Ti^{3+} to Ti^{4+},[40] one concludes that among the three catalysts, the CuCe/Ti catalyst may have the highest catalytic activity.

The surface morphology in Figure 4 shows that the surfaces of Cu/Ti and Ce/Ti catalysts are loose, the regularity of morphology is poor, and the particle size distribution is not uniform enough; however, the CuCe/Ti catalyst has a smoother surface and more uniform particle size distribution. The above three characterization results indicated that CuCe/Ti may have better catalytic performance.[41−43] Therefore, in this work, we selected CuCe/Ti as the catalyst and cooperated with the DBD reactor to oxidize Hg^0.

3.2. Effects of O_2 Content and Discharge Voltage on η_{Hg}. The energy density can be calculated by SED (J/L) = P (J/s)/Q (L/min) × 60 s/min, in which P represents the power consumed and Q represents the flow of gas.[33] We recorded the voltage and current data from the oscilloscope. The relationship between energy density and voltage thus obtained is shown in Figure 5, indicating that when the voltage increased from 3 to 7.5 kV, SED only slightly increased from 4.6 to 7.8 J/L. When the voltage was within the range of 8−10 kV, SED increased rapidly from 38.1 to 48.5 J/L. When the voltage continued to increase, SED increased faster.

O_3 and free radicals are produced during the DBD discharge, as shown in eqs 1−4. Figure 6 shows the effect of the O_2 content on the η_{Hg} at different discharge voltages. In the range of 3−8 kV, the variation of the Hg^0 content was very small, so it is not plotted in Figure 6.

The reason for this can be explained in Figure 5. When the voltage was less than 8 kV, the change in energy density was small, so the number of generated free radicals was small and the η_{Hg} low. When the voltage was greater than 8 kV, the energy density increased rapidly as the voltage increased, and the η_{Hg} also increased rapidly. When the discharge voltage was constant, the higher the O_2 content, the higher the collision probability of O_2 and higher the energy of the electrons, thus more O_3 and $^\bullet O$ were generated to participate in the reaction, and the η_{Hg} was increased. For the four kinds of O_2 contents,

Figure 2. X-ray diffraction patterns of catalysts.
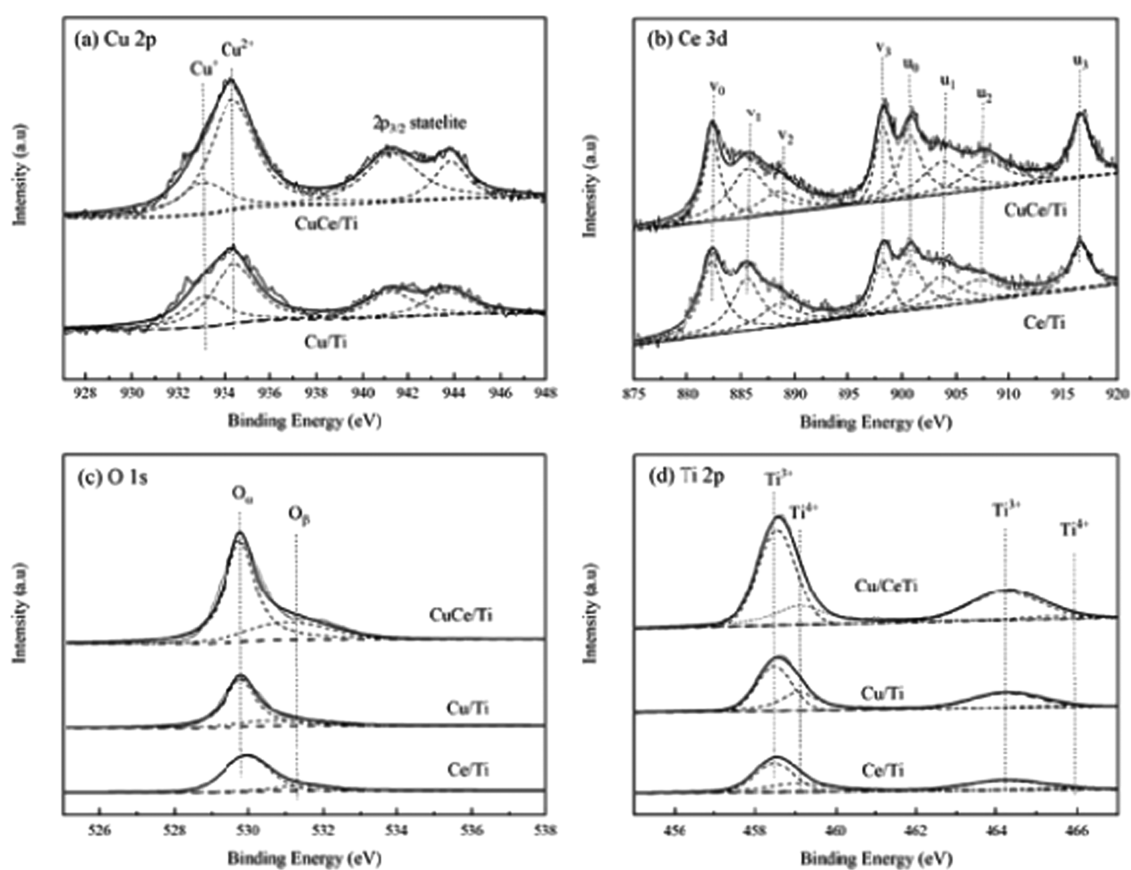
Figure 3. X-ray photoelectron energy spectrum analysis of the catalysts: (a) Cu 2p, (b) Ce 3d, (c) O 1s, and (d) Ti 2p.
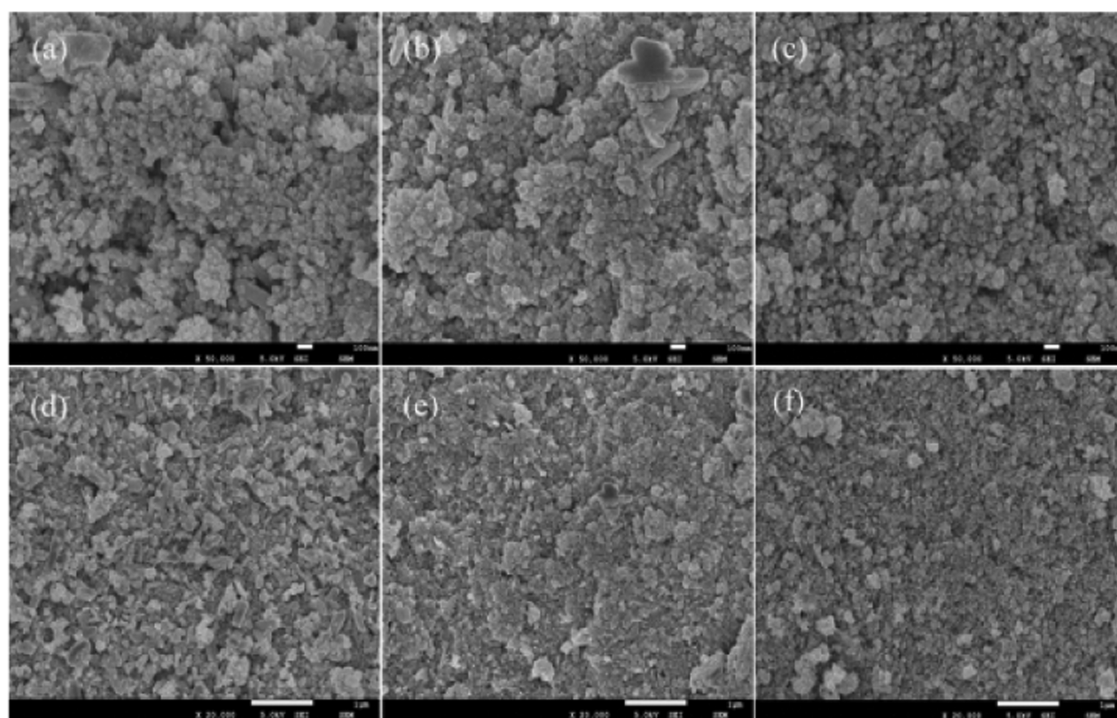

Figure 4. Scanning electron microscope analysis of the catalysts: (a) Cu/Ti (50 000:1); (b) Ce/Ti (50 000:1); (c) CuCe/Ti (50 000:1); (d) Cu/Ti (20 000:1); (e) Ce/Ti (20 000:1); and (f) CuCe/Ti (20 000:1).

the η_{Hg} reached the maximum (85.1, 90.7, 93.5, and 96.5%, respectively) in the range of 9.5−10 kV. In the case of too high voltage, because N_2 in the flue gas as the carrier gas and

its content far exceeds O_2, a large amount of $^\bullet N$ produced by high-voltage discharge would preferentially consume O_3 and $^\bullet O$, resulting in a decrease in the η_{Hg}. Moreover, in the case of
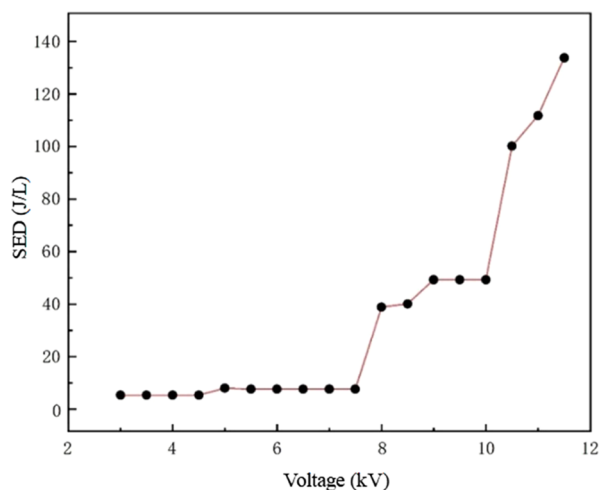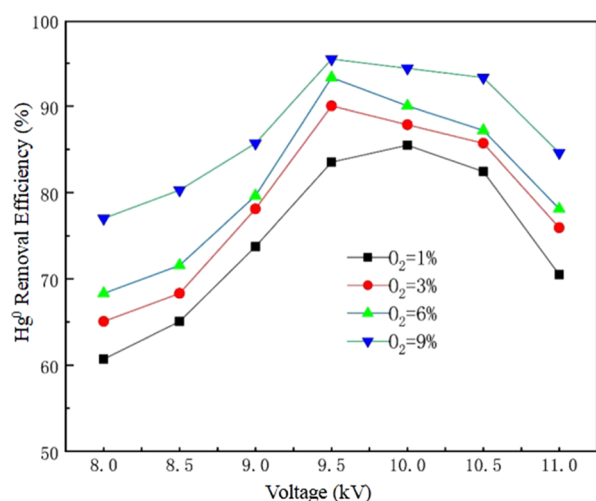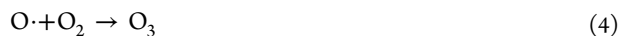
Figure 5. Voltage dependence of SED.

Figure 6. O_2 content dependence of η_{Hg} at different discharge voltages.

too high voltage, part of HgO (as shown in eqs 5 and 6) adsorbed on the inner wall of the quartz tube would be reduced to elemental mercury under the influence of discharge arc, thus reducing the η_{Hg}.

$$e + O_2 \rightarrow O\cdot + O\cdot \tag{1}$$

$$e + N_2 \rightarrow N\cdot + N\cdot \tag{2}$$

$$N\cdot + O_2 \rightarrow NO + O\cdot \tag{3}$$

$$O\cdot + O_2 \rightarrow O_3 \tag{4}$$

$$Hg^0 + O\cdot \rightarrow HgO \tag{5}$$

$$Hg^0 + O_3 \rightarrow HgO + O_2 \tag{6}$$

3.3. Effects of NO, SO$_2$, and H$_2$O(g) on η_{Hg}. The composition of flue gas is very complex, including O_2, CO_2, N_2, SO_2, NO_x, H_2O, and HCl. When DBD is used to treat flue gas, multiple components can react with high-energy electrons to generate different active substances and free radicals and undergo redox reactions with O_3 and $^\bullet O$, thereby affecting the conversion of Hg^0. In this section, we used the controlled

variable method to study the influences of NO, SO_2, and H_2O(g) on the η_{Hg}.

NO will be oxidized by active materials and affect the η_{Hg}. An et al.[44] found that the presence of NO will reduce the η_{Hg} because the reaction rate constant of the reaction of NO and O_3 was much greater than that of NO and Hg^0, so NO would compete with Hg^0 for active substances. However, some others[27,34] believed that NO provides additional O atoms to increase the active materials and promote the oxidation of Hg^0. The NO concentration dependence of η_{Hg} was shown in Figure 7 (O_2 concentration was 6%).
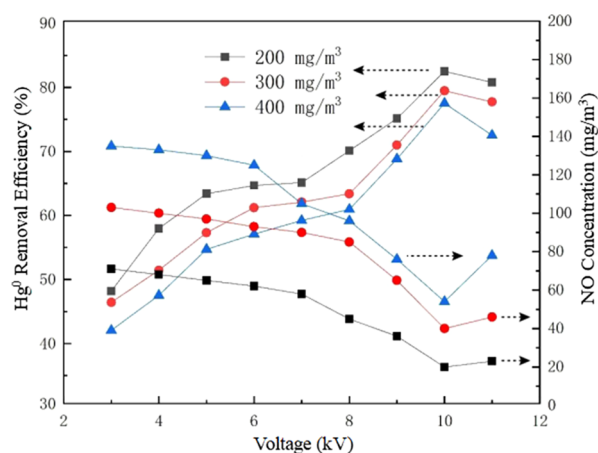

Figure 7. NO concentration dependence of η_{Hg}.

The experimental results supported the conclusion of An et al.[44] that increasing NO would reduce the η_{Hg}. The η_{Hg} showed an upward trend with the increase of voltage and reached the maximum at 10 kV. The concentration of NO at the outlet also reached the minimum value at 10 kV, which proved that NO also participates in the reaction and is converted during the DBD discharge process. The main reactions in the DBD reactor include eqs 7−9[45−47]

$$NO + O\cdot \rightarrow NO_2 \tag{7}$$

$$NO + O_3 \rightarrow NO_2 + O_2 \tag{8}$$

$$NO_2 + O_3 \rightarrow NO_3 + O_2 \tag{9}$$

The effect of SO_2 concentration on η_{Hg} is shown in Figure 8 (O_2 concentration was 6%).

Different from Figure 6, the η_{Hg} quickly reached about 95% in the range of 3−8 kV, and the concentration of SO_2 at the outlet also decreased continuously with the increase in voltage. Wang et al.[48] found that SO_2 consumes O atoms and inhibits the conversion of Hg^0. However, some researchers[20,24,33] believed that SO_2 is mainly oxidized by $^\bullet OH$ and $^\bullet O$ to HSO_3^- and SO_3, which had little effect on the conversion of Hg^0. Through our experimental data, we found that the generated HSO_3^- and SO_3 react with HgO to generate $HgSO_4$, thereby oxidizing part of Hg^0. The main reactions include eqs 10−13; however, there is still controversy about how SO_2 affects the oxidation of Hg^0.[49,50]
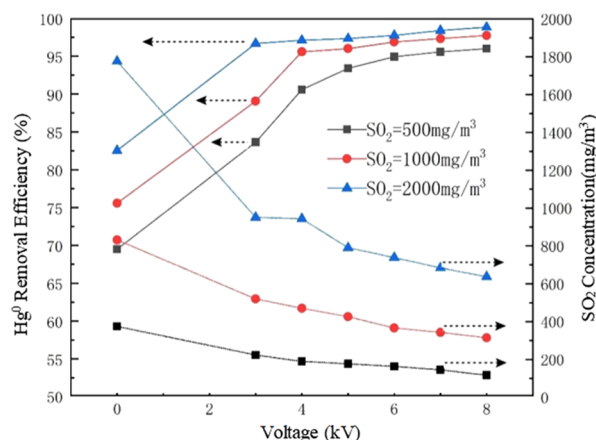
$$SO_2 + O\cdot \rightarrow SO_3 \tag{10}$$

$$HgO + SO_3 \rightarrow HgSO_4 \tag{11}$$

$$Hg^0 + O\cdot \rightarrow HgO \tag{12}$$

Figure 8. SO_2 concentration dependence of η_{Hg}.

$$Hg^0 + O_3 \rightarrow HgO + O_2 \tag{13}$$

To clarify the effect of $H_2O(g)$ content on the η_{Hg}, we generated a certain amount of water vapor by bubbling and heating, and introduced the water vapor into the DBD reactor through N_2, and obtained the corresponding absolute humidity based on the flow rate. The result is shown in Figure 9 (O_2 concentration was 6%).
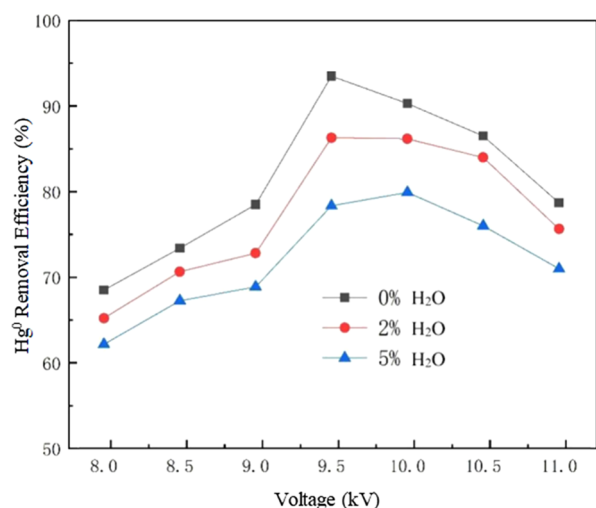

Figure 9. Water content dependence of η_{Hg}.

When there was no H_2O in the reactor, the η_{Hg} reached a peak of 93.5% at 9.5 kV. When there was H_2O, the η_{Hg} decreased with the increase in $H_2O(g)$. The chemical process in the DBD reactor is shown in eqs 14−17, indicating that water vapor can consume part of O_3, thereby inhibiting the oxidation of Hg^0[44]

$$H_2O + O_3 \rightarrow H_2O_2 + O_2 \tag{14}$$

$$H_2O_2 \rightarrow OH \cdot + OH \cdot \tag{15}$$

$$Hg^0 + OH \cdot \rightarrow Hg(OH)_2 \tag{16}$$

$$Hg^0 + O_3 \rightarrow HgO + O_2 \tag{17}$$

The effect of the coexistence of NO and SO_2 on the η_{Hg} was shown in Figure 10. Under 6% O_2 concentration, the η_{Hg} was the highest when only SO_2 was present, which can reach
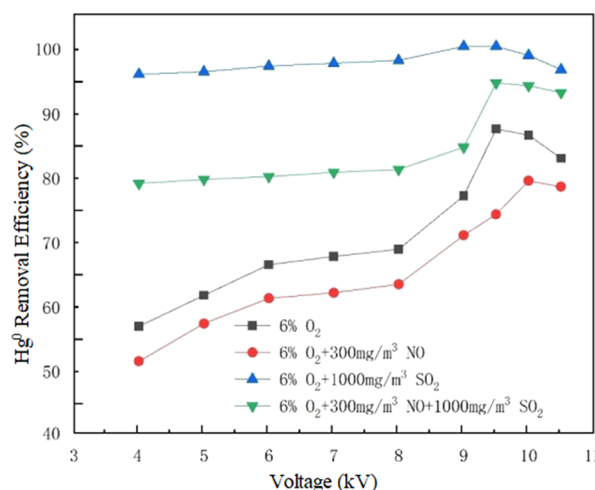

Figure 10. NO and SO_2 concentrations dependences of η_{Hg}.

95.6% at 4 kV and 100% at 9 kV. The η_{Hg} was the lowest when only NO was present, which indicated again that SO_2 promotes the oxidation of Hg^0, while NO inhibits the oxidation of Hg^0. When the inlet gas was composed of 70 $\mu g/m^3$ Hg^0 + 6% O_2 + 300 mg/m^3 NO + 1000 mg/m^3 SO_2, a η_{Hg} of 93% was achieved at 9.5 kV. However, adding $H_2O(g)$ to this inlet gas would reduce the η_{Hg}. For example, when the 2% H_2O was introduced in the above inlet gas, the η_{Hg} rapidly dropped from 93 to 86.3%; when the introduced H_2O content was 5%, the η_{Hg} dropped to 79.9%. Therefore, it is best to conduct dehydration first when using DBD-CuCe/Ti reactor to oxidize Hg^0 or simultaneously oxidize multiple pollutants in the flue gas. Besides, the flue gas HCl affects the redox reaction, although the chemical properties of the flue gas CO_2 are very stable, the concentration of CO_2 is relatively high. Hence, it is necessary to investigate the influence of HCl and CO_2 on the oxidation of multipollutants in future work.

4. CONCLUSIONS

To efficiently oxidize Hg^0 in the flue gas, we prepared the CuCe/Ti catalyst and proposed a new method of DBD coupling the CuCe/Ti catalytic oxidation. The experiment showed that DBD coupling CuCe/Ti can lead to high η_{Hg}, so it has great application potential. Our results showed that

(1) the oxides of Cu−Ce had higher catalytic activity than the single metal oxides;

(2) when the discharge voltage was about 9.5 kV, the maximum η_{Hg} reached 93%, which means both the energy density and η_{Hg} were satisfactory;

(3) the oxidation of Hg^0 was mainly due to the oxidation from $\cdot$O, $\cdot$OH, and O_3, but the intermediate products also affected the η_{Hg}; and

(4) O_2 and SO_2 were favorable for the oxidation of Hg^0, but increasing NO and H_2O tended to decrease η_{Hg}.

■ AUTHOR INFORMATION

Corresponding Author

Pan Zhang − *Hebei Provincial Key Laboratory of Power Plant Flue Gas Multi-Pollutants Control, Department of Environmental Science and Engineering, North China Electric Power University, Baoding 071003, P. R. China;* orcid.org/0000-0003-2620-5197; Phone: 86-312-7525517; Email: zhangpan01@ncepu.edu.cn

Authors

Yujie Liao − *Hebei Provincial Key Laboratory of Power Plant Flue Gas Multi-Pollutants Control, Department of Environmental Science and Engineering, North China Electric Power University, Baoding 071003, P. R. China*

Zhong Zhong − *Hebei Provincial Key Laboratory of Power Plant Flue Gas Multi-Pollutants Control, Department of Environmental Science and Engineering, North China Electric Power University, Baoding 071003, P. R. China*

Shaoping Cui − *Hebei Provincial Key Laboratory of Power Plant Flue Gas Multi-Pollutants Control, Department of Environmental Science and Engineering, North China Electric Power University, Baoding 071003, P. R. China;* ⬤ orcid.org/0000-0002-9991-1837

Dong Fu − *Hebei Provincial Key Laboratory of Power Plant Flue Gas Multi-Pollutants Control, Department of Environmental Science and Engineering, North China Electric Power University, Baoding 071003, P. R. China*

Complete contact information is available at:
https://pubs.acs.org/10.1021/acsomega.0c05859

Notes

The authors declare no competing financial interest.

◼ REFERENCES

(1) Kershaw, T. G.; Clarkson, T. W.; Dhahir, P. H. The Relationship Between Blood Levels and Dose of MeHg in Man. *Arch. Environ. Health* **1980**, *35*, 28−36.

(2) Pacyna, E. G.; Pacyna, J. M.; Sundseth, K.; Munthe, J.; Kindbom, K.; Wilson, S.; Steenhuisen, F.; Maxson, P. Global emission of mercury to the atmosphere from anthropogenic sources in 2005 and projections to 2020. *Atmos. Environ.* **2010**, *44*, 2487−2499.

(3) Feng, X.; Streets, D.; Hao, J.; Wu, Y.; Li, G. Mercury Emissions from Industrial Sources in China. In *Mercury Fate and Transport in the Global Atmosphere*; Springer: Boston, MA, 2009; pp 67−79.

(4) Akers, D.; Raleigh, C. The Mechanisms of Trace Element Removal During Coal Cleaning. *Coal Prep.* **1998**, *19*, 257−269.

(5) Wu, Q.; Wang, S.; Li, G.; Liang, S.; Lin, C.; Wang, Y.; Cai, S.; Liu, K.; Hao, J. Temporal Trend and Spatial Distribution of Speciated Atmospheric Mercury Emissions in China During 1978-2014. *Environ. Sci. Technol.* **2016**, *50*, 13428−13435.

(6) Luo, G.; Yao, H.; Xu, M.; Gupta, R.; Xu, Z. Identifying modes of occurrence of mercury in coal by temperature programmed pyrolysis. *Proc. Combust. Inst.* **2011**, *33*, 2763−2769.

(7) Wdowin, M.; Wiatros-Motyka, M. M.; Panek, R.; Stevens, L. A.; Franus, W.; Snape, C. E. Experimental study of mercury removal from exhaust gases. *Fuel* **2014**, *128*, 451−457.

(8) Wang, B.; Xu, X.; Xu, W.; Wang, N.; Xiao, H.; Sun, Y.; Huang, H.; Yu, L.; Fu, M.; Wu, J.; et al. The Mechanism of Non-thermal Plasma Catalysis on Volatile Organic Compounds Removal. *Catal. Surv. Asia* **2018**, *22*, 73−94.

(9) Subrahmanyam, C.; Magureanu, M.; Renken, A.; Kiwi-Minsker, L. Catalytic abatement of volatile organic compounds assisted by non-thermal plasma: Part 1. A novel dielectric barrier discharge reactor containing catalytic electrode. *Appl. Catal., B* **2006**, *65*, 150−156.

(10) Guo, Q.; With, P.; Liu, Y.; Gläser, R.; Liu, C. Carbon template removal by dielectric-barrier discharge plasma for the preparation of zirconia. *Catal. Today* **2013**, *211*, 156−161.

(11) Wang, J.; Wang, W.; Xu, W.; Wang, X.; Zhao, S. Mercury removals by existing pollutants control devices of four coal-fired power plants in China. *J. Environ. Sci.* **2011**, *23*, 1839−1844.

(12) Liu, L.; Zheng, C.; Wu, S.; Gao, X.; Ni, M.; Cen, K. Manganese-cerium oxide catalysts prepared by non-thermal plasma for NO oxidation: Effect of O_2 in discharge atmosphere. *Appl. Surf. Sci.* **2017**, *416*, 78−85.

(13) Niu, Q.; Luo, J.; Xia, Y.; Sun, S.; Chen, Q. Surface modification of bio-char by dielectric barrier discharge plasma for Hg^0 removal. *Fuel Process. Technol.* **2017**, *156*, 310−316.

(14) Liu, Y.; Wang, Y.; Wang, H.; Wu, Z. Catalytic oxidation of gas-phase mercury over Co/TiO_2 catalysts prepared by sol−gel method. *Catal. Commun.* **2011**, *12*, 1291−1294.

(15) Byun, Y.; Koh, D. J.; Shin, D. N. Removal mechanism of elemental mercury by using non-thermal plasma. *Chemosphere* **2011**, *83*, 69−75.

(16) Ma, H.; Chen, P.; Zhang, M.; Lin, X.; Ruan, R. Study of SO_2 Removal Using Non-thermal Plasma Induced by Dielectric Barrier Discharge (DBD). *Plasma Chem. Plasma Process.* **2002**, *22*, 239−254.

(17) Wang, T.; Liu, H.-Z.; Yang, B.; Sun, B.-M.; Xiao, H.-P.; Zhang, Y. Effect of plasma-catalyst system on NO removal using M−Cu (M = Mn, Ce, Cr, Co, and Fe) catalysts. *Jpn. J. Appl. Phys.* **2016**, *55*, No. 116202.

(18) Shen, Y.; Zong, Y.; Ma, Y.; Zhu, S.; Jin, Q. Synergistic catalytic removals of NO, CO and C_3H_8 over $CeSn_{0.8}W_{0.6}O_x/TiAl_{0.2}Si_{0.1}O_x$. *Fuel* **2016**, *180*, 727−736.

(19) Piumetti, M.; Fino, D.; Russo, N. Mesoporous manganese oxides prepared by solution combustion synthesis as catalysts for the total oxidation of VOCs. *Appl. Catal., B* **2015**, *163*, 277−287.

(20) Zhang, X.; Wang, J.; Tan, B.; Zhang, N.; Bao, J.; He, G. Ce-Co interaction effects on the catalytic performance of uniform mesoporous Ce_x-Co_y catalysts in Hg^0 oxidation process. *Fuel* **2018**, *226*, 18−26.

(21) Tian, W.; Yang, H.; Fan, X.; Zhang, X. Catalytic reduction of NO_x with NH_3 over different-shaped MnO_2 at low temperature. *J. Hazard. Mater.* **2011**, *188*, 105−109.

(22) Li, L.; Shen, Q.; Cheng, J.; Hao, Z. Catalytic oxidation of NO over TiO_2 supported platinum clusters I. Preparation, characterization and catalytic properties. *Appl. Catal., B* **2010**, *93*, 259−266.

(23) Li, P.; Chen, X.; Li, Y.; Schwank, J. W. Effect of preparation methods on the catalytic activity of $La_{0.9}Sr_{0.1}CoO_3$ perovskite for CO and C_3H_6 oxidation. *Catal. Today* **2020**, DOI: 10.1016/j.cattod.2020.03.012.

(24) An, J.; Lou, J.; Meng, Q.; Zhang, Z.; Ma, X.; Li, J. Non-thermal plasma injection-CeO_2-WO_3/TiO_2 catalytic method for high-efficiency oxidation of elemental mercury in coal-fired flue gas. *Chem. Eng. J.* **2017**, *325*, 708−714.

(25) Ouyang, B.; Zhang, Y.; Zhang, Z.; Fan, H. J.; Rawat, R. S. Nitrogen-Plasma-Activated Hierarchical Nickel Nitride Nanocorals for Energy Applications. *Small* **2017**, *13*, No. 1604265.

(26) Zhang, Y.; Ouyang, B.; Xu, J.; Jia, G.; Chen, S.; Rawat, R. S.; Fan, H. J. Rapid Synthesis of Cobalt Nitride Nanowires: Highly Efficient and Low-Cost Catalysts for Oxygen Evolution. *Angew. Chem., Int. Ed.* **2016**, *55*, 8670−8674.

(27) Huang, C.; Bai, S.; Lv, J.; Li, Z. Characterization of Silica-Supported Cobalt Catalysts Prepared by Decomposition of Nitrates Using Dielectric-Barrier Discharge Plasma. *Catal. Lett.* **2011**, *141*, 1391−1398.

(28) Sousa, J. P. S.; Pereira, M. F. R.; Figueiredo, J. L. Catalytic oxidation of NO to NO_2 on N-doped activated carbons. *Catal. Today* **2011**, *176*, 383−387.

(29) Cui, S.; Hao, R.; Fu, D. An integrated system of dielectric barrier discharge combined with wet electrostatic precipitator for simultaneous removal of NO and SO_2: Key factors assessments, products analysis and mechanism. *Fuel* **2018**, *221*, 12−20.

(30) Cui, S.; Hao, R.; Fu, D. Integrated method of non-thermal plasma combined with catalytical oxidation for simultaneous removal of SO_2 and NO. *Fuel* **2019**, *246*, 365−374.

(31) Cui, S.; Zhong, Z.; Liao, Y.; Qi, L.; Fu, D. Simultaneous Removal of NO and SO_2 via an Integrated System of Nonthermal Plasma Combined with Catalytic Oxidation and Wet Electrostatic Precipitator. *Energy Fuels* **2019**, *33*, 10078−10089.

(32) Zhang, J.; Duan, Y.; Zhao, W.; Zhu, C.; Zhou, Q.; Ding, W. Study on Elemental Mercury Oxidation by Non-thermal Plasma with Calcium Chloride Enhancement. *Plasma Chem. Plasma Process.* **2018**, *38*, 573−586.

(33) Zhang, J.; Duan, Y.; Zhao, W.; Zhu, C.; Zhou, Q.; She, M. Removal of Elemental Mercury from Simulated Flue Gas by Combining Non-thermal Plasma with Calcium Oxide. *Plasma Chem. Plasma Process.* **2016**, *36*, 471−485.

(34) Gao, X.; Liu, S.; Zhang, Y.; Luo, Z.; Cen, K. Physicochemical properties of metal-doped activated carbons and relationship with their performance in the removal of SO_2 and NO. *J. Hazard. Mater.* **2011**, *188*, 58−66.

(35) Zhong, L.; Cai, W.; Yu, Y.; Zhong, Q. Insights into synergistic effect of chromium oxides and ceria supported on Ti-PILC for NO oxidation and their surface species study. *Appl. Surf. Sci.* **2015**, *325*, 52−63.

(36) Li, X.; Zhang, S.; Jia, Y.; Liu, X.; Zhong, Q. Selective catalytic oxidation of NO with O_2 over Ce-doped MnO_x/TiO_2 catalysts. *J. Nat. Gas Chem.* **2012**, *21*, 17−24.

(37) Wang, M.; Liu, H.; Huang, Z.-H.; Kang, F. Activated carbon fibers loaded with MnO_2 for removing NO at room temperature. *Chem. Eng. J.* **2014**, *256*, 101−106.

(38) Liu, L.; Yao, Z.; Liu, B.; Dong, L. Correlation of structural characteristics with catalytic performance of $CuO/Ce_xZr_{1−x}O_2$ catalysts for NO reduction by CO. *J. Catal.* **2010**, *275*, 45−60.

(39) Pang, L.; Fan, C.; Shao, L.; Song, K.; Yi, J.; Cai, X.; Wang, J.; Kang, M.; Li, T. The Ce doping Cu/ZSM-5 as a new superior catalyst to remove NO from diesel engine exhaust. *Chem. Eng. J.* **2014**, *253*, 394−401.

(40) Xiong, Y.; Tang, C.; Yao, X.; Zhang, L.; Li, L.; Wang, X.; Deng, Y.; Gao, F.; Dong, L. Effect of metal ions doping (M=Ti^{4+}, Sn^{4+}) on the catalytic performance of MnO_x/CeO_2 catalyst for low temperature selective catalytic reduction of NO with NH_3. *Appl. Catal., A* **2015**, *495*, 206−216.

(41) Liu, L.; Gao, X.; Song, H.; Zheng, C. H.; Zhu, X.-B.; Luo, Z.-Y.; Ni, M.-J.; Chen, K.-F. Study of the promotion effect of Iron on supported manganese catalysts for NO Oxidation. *Aerosol Air Qual. Res.* **2014**, *14*, 1038−1046.

(42) Cai, W.; Zhao, Y.; Chen, M.; Jiang, X.; Wang, H.; Ou, M.; Wan, S.; Zhong, Q. The formation of 3D spherical Cr-Ce mixed oxides with roughness surface and their enhanced low-temperature NO oxidation. *Chem. Eng. J.* **2018**, *333*, 414−422.

(43) Yang, Z.; Li, H.; Liu, X.; Li, P.; Yang, J.; Lee, P.-H.; Shih, K. Promotional effect of CuO loading on the catalytic activity and SO_2 resistance of $MnOx/TiO_2$ catalyst for simultaneous NO reduction and Hg^0 oxidation. *Fuel* **2018**, *227*, 79−88.

(44) An, J.; Shang, K.; Lu, N.; Jiang, Y.; Wang, T.; Li, J.; Wu, J. Oxidation of Elemental Mercury by Active Species Generated From a Surface Dielectric Barrier Discharge Plasma Reactor. *Plasma Chem. Plasma Process.* **2014**, *34*, 217−228.

(45) Liu, K.; Zheng, Z.; Liu, S.; Hu, Y. Study on the Physical and Chemical Characteristics of DBD: The Effect of N_2/O_2 Mixture Ratio on the Product Regulation. *Plasma Chem. Plasma Process.* **2019**, *39*, 1255−1274.

(46) Majumdar, A.; Singh, R. K.; Palm, G. J.; Hippler, R. Dielectric barrier discharge plasma treatment on *E. coli*: Influence of CH_4/N_2, O_2, N_2/O_2, N_2, and Ar gases. *J. Appl. Phys.* **2009**, *106*, No. 084701.

(47) Zhang, Y.; Tang, X.; Yi, H.; Yu, Q.; Wang, J.; Gao, F.; Gao, Y.; Li, D.; Gao, Y. The byproduct generation analysis of the NO_x conversion process in dielectric barrier discharge plasma. *RSC Adv.* **2016**, *6*, 63946−63953.

(48) Wang, Z. H.; Jiang, S. D.; Zhu, Y. Q.; Zhou, J. S.; Zhou, J. H.; Li, Z. S.; Cen, K. F. Investigation on elemental mercury oxidation mechanism by non-thermal plasma treatment. *Fuel Process. Technol.* **2010**, *91*, 1395−1400.

(49) Luo, J.; Niu, Q.; Xia, Y.; Cao, Y.; Du, R.; Sun, S.; Lu, C. Investigation of Gaseous Elemental Mercury Oxidation by Non-thermal Plasma Injection Method. *Energy Fuels* **2017**, *31*, 11013−11018.

(50) Zhang, Y.; Zhang, Y.; Wang, T.; Lin, J.; Romero, C. E.; Pan, W. Oxidation of elemental mercury with non-thermal plasma coupled with a wet process. *Fuel* **2017**, *197*, 320−325.